

# Longitudinal Trajectory Forecasting of Human-driven Vehicles Near Traffic Lights Using Vehicle Communications

Geunseob (GS) Oh and Huei Peng

**Abstract**—Forecasting trajectories of human-driven vehicles is a crucial problem in autonomous driving. Trajectory forecasting in the urban area is particularly hard due to complex interactions with actors (cars and pedestrians), and traffic lights (TLs). Unlike the former that has been actively studied, the impact of TLs on the prediction has rarely been discussed. Inspired by the fact that human drives differently depending on phases (green, yellow, red) and timings (elapsed time), we propose a novel approach to the trajectory forecasting problem. In our approach, we take the states of TLs as part of the conditional inputs to our deep-learning models (*Human Policy Models*) which map a sequence of a vehicle’s states and a context to a subsequent action (longitudinal acceleration) of the vehicle. Trained on real-world naturalistic driving data recorded near a signalized intersection over 2 years, the models learn how human drivers react to various states of TLs. These *Human Policy Models* are then used in trajectory forecasting; the key idea is to utilize the future phases and timings of TLs obtained through vehicle-to-infrastructure communications. Accordingly, an ablation study is presented to show that utilization of the phases and timings of TL significantly improves the accuracy of the forecasts. Finally, our probabilistic *Human Policy Models* provides probabilistic contexts for the forecasts and captures competing policies, for example, *pass* or *stop* in the yellow-light dilemma zone.

## I. INTRODUCTION

Autonomous driving has been more successful in highway than in urban city mainly due to the simplicity of its driving environment; absence of traffic signals, and more stable interactions with other vehicles. Realizing fully autonomous vehicles in urban driving environments is more challenging due to the existence of traffic signals, and frequent interactions with human-driven vehicles.

One of the major differences between urban city and highway driving is traffic lights (TLs). In urban areas, especially in the vicinity of TLs exemplified by signalized corridors or intersections, the motions of vehicles are mainly governed by traffic signals. People drive in such a manner that they obey the traffic signals and properly respond to implicit rules imposed by traffic lights. Examples of the implicit traffic rules include stopping before a traffic light in a red phase, maintaining a proper speed in a green phase in a free-flow situation. This is why predicting how human drivers respond to traffic signals is the key to successful autonomous driving. If we can accurately predict the trajectories of surrounding human-driven vehicles, then we can leverage such predictions in decision-making, trajectory planning, and control synthesis of a self-driving vehicle.

Geunseob (GS) Oh and Huei Peng are with the Department of Mechanical Engineering, University of Michigan, Ann Arbor, MI 48109 USA, Email : {gsoh, hpeng}@umich.edu

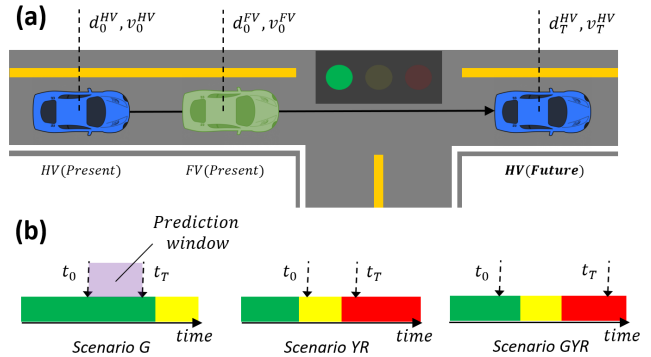


Fig. 1. (a) The longitudinal trajectory forecasting problem near a traffic light for the vehicles with *through* moves is depicted. Given a sequence of past states (positions and speeds) of a host vehicle (HV) and contexts (TLs, its front vehicle (FV)), our goal is to forecast HV’s states under various states of TLs. (b) Three example scenarios of the problem are described. The full list of the scenarios is described in Table. I. We define scenario G as a forecasting problem when the prediction window starts on a green light and ends on the same green light. Scenario GYR represents a forecasting problem where the window spans over a set of green, yellow, and red lights. All the other scenarios are defined likewise.

Recent studies in trajectory forecasting have been focusing on accurate modeling of the interactions among road agents [1], and/or applying generative models in predictions such as *generative adversarial networks* (GAN) [2] and *flow* [3]. For pedestrian trajectory forecasting, researchers have approached the problem utilizing convolutional & recurrent neural nets [4], [5], and generative models like GAN [6]. Despite the important role of TLs in governing vehicle trajectories, the dynamics between TLs and vehicle trajectories has rarely been discussed in trajectory forecasting literature.

It is further elaborated in Fig. 2, which describes the less recognized, perhaps overlooked, impact of TLs in trajectory forecasting. Fig. 2 demonstrates how the states of TLs affect vehicle trajectories, and how the uncertainty in the states of TLs can cause high prediction errors. Even for models that are carefully designed to account for the uncertainty in the future phase and to output multi-modal predictions for the two possibilities (a case where the phase remained red, the other case where the phase shifted to green) (Fig. 2), the question still remains: precisely when will the phase shift?

On the other hand, there have been efforts to model the dynamic impact of TLs in the transportation research community. However, there is no comprehensive model which describes the behavior of human drivers near traffic signals available yet. A few papers have studied specific instances of the dynamics but limited to a few simple scenarios; [7],

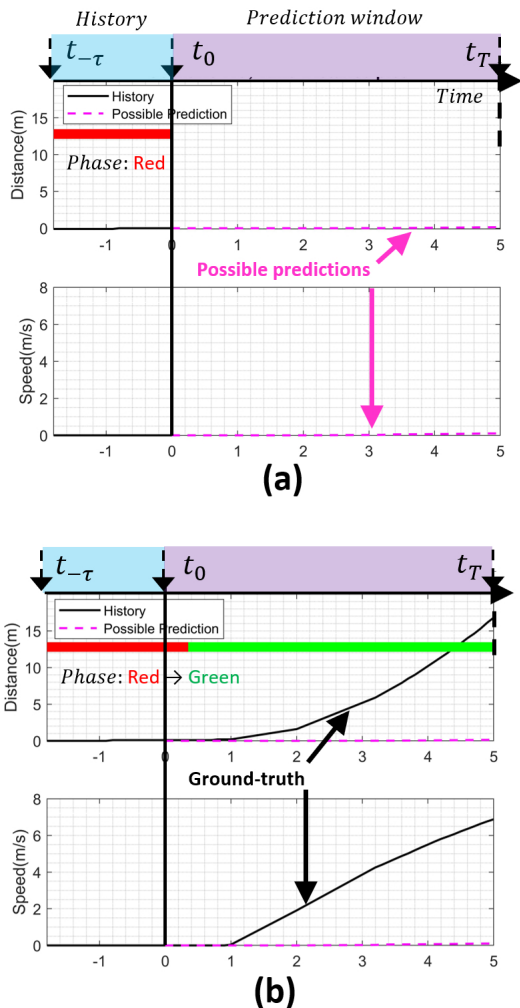


Fig. 2. A motivational example sampled from our real-world dataset is depicted to demonstrate how uncertainty in the states of TLs makes the forecast hard. The sample is a 7s long RG scenario, where the first 2s is the history observed, and the last 5s is the future yet hasn't been seen. The goal is to predict *longitudinal* position and speed of a vehicle. We define 0m as the position of the vehicle at  $t = 0s$ . The distance to a TL is then 13m. (a) Given the history of the vehicle's position and the speed, the red phase observed at  $t = 0s$ , and that we are uncertain about the traffic phase at  $t > 0s$ , a reasonable prediction that an existing method would make is to predict the vehicle to stay put (pink dotted line). (b) However, in reality, the phase shifted to green at  $t = 0.35s$ , and the vehicle sped away as depicted as black line, resulting in greater prediction errors in both position and speed.

[8], and [9] developed models for vehicles approaching a signalized intersection and making complete stops in red light. [9], [10], [11], [12], and [13] proposed models for vehicles departing from a signalized intersection from zero-speed in green phase. However, these models are either limited to specific instances of the problem, or they can not serve as a forecasting model since they require parameters like total deceleration time, final speed, which can only be measured after a trip is complete. A group of papers [14], and [15] presented prediction algorithms for the vehicles in highway and in car-following scenarios [16] based on car models proposed in [17], and [18]. These models, however, do not describe how human drivers react to the traffic signals.

In order to leverage the rich information that comes from the dynamics between TLs and human drivers, and to apply the dynamics to the trajectory forecasting problem, our idea is to simply utilize vehicle-to-infrastructure (V2I) communications. By communicating with TL controllers using V2I communication, one can access **the future profile** of the TLs ahead of time. Based on the idea, we demonstrate how access to the future profile of the TLs can improve the accuracy of the trajectory forecasts.

In this paper, we first propose two models which map a sequence of states of a human-driven vehicle, its front vehicle and the corresponding traffic signal phase and timing (SPaT) information to the subsequent action (longitudinal acceleration) that the vehicle takes. We name the models "Human Policy Models" to highlight that the models return an action given input states. The first model is a deterministic human policy model which returns the most-probable action, and the second model is a probabilistic human policy model which outputs distribution parameters. Then, we utilize these models to forecast longitudinal trajectories of cars near TLs over a time span. We take a data-driven approach to obtain the human policy models using LSTM and mixture density networks (MDN) [19]. For the training, validation, and testing, we used 502,253 sequences excerpted from naturalistic (non-obstructive, uncontrolled) trips from 50 distinct cars over 2 years at a signalized intersection in Ann Arbor, MI.

The remainder of the paper is organized as follows: Section II elaborates on the proposed human policy models. Section III describes the framework which describes how we forecast trajectories using the human policy models. Section IV describes prediction results obtained from the models. Finally, Section V offers concluding remarks.

## II. HUMAN POLICY MODEL

### A. Problem Description

Our goal is to forecast longitudinal trajectories of human-driven vehicles at the vicinity of TL(s), focusing on the *through* vehicles which passed through a signalized corridor or intersection, specifically, under the diverse scenarios depicted in Fig. 1 with different phases and timings of TLs. This problem has not only been rarely discussed but also is challenging due to stochastic reactions of human drivers to SPaT. For example, a driver may prefer hard-braking when he/she approaches to a red light, while others prefer soft-braking. Also, the reactions of drivers at steady phases (Green(G), Yellow(Y), Red(R)) are different from those at phase transitions (GY, YR, RG). Another motivational example is the decision making in yellow light dilemma zone [20], where a driver arrives at a TL at a high speed. There usually exists two competing decisions; a driver could either make a sudden stop or pass through the traffic light.

In this sense, we break the problem down to seven distinct scenarios which are depicted in Fig. 1(b) and Table. I. The idea behind this categorization is our belief that humans react differently at different SPaT, resulting in the trajectories to be significantly different per scenario; thus, a model should be validated against all the 7 scenarios.

## B. Related Works

To the authors' best knowledge, we are not aware of literature which tackles this particular forecasting problem in the machine learning community. In traditional transportation community, a few papers have discussed acceleration models or velocity profiles near traffic signals. [9], [12], [11], and [13] proposed polynomial velocity & acceleration models for vehicles departing from a signalized intersection from zero-speed in green lights. [7], [8], and [9] developed deceleration models for vehicles approached a TL which make complete stops in red light. However, these models only studied very specific instances of the problem. We classified the available studies into the scenarios we defined in Table. I.

TABLE I  
Seven distinct scenarios of the prediction problem

Scenario	Available Studies in Transportation Community
G	D0(departure from zero-speed) ATL Newzealand(1990), Bham(2002), Day(2013), Modified IDM(2018)
	General None
Y	None
R	A0(arrival to zero-speed) Bennett(1995), Wang(2005), Modified IDM(2018)
	General None
GY	None
YR	None
RG	None
GYR	None

We believe that a comprehensive model which describes the behavior of human drivers in all scenarios described in Fig. 1(b) and Table. I is crucial to accurately forecast trajectories of human vehicles near traffic lights. To the best of our knowledge, there is no such model available yet.

## C. Proposed Model

The key intuition behind modeling a driver's reaction to TL is to utilize the states of a TL, specifically phase (G,Y,R), and timing (time elapsed in the current phase). Accordingly, we propose "Human Policy Models" which map a sequence of past states of a host vehicle ( $X_{t-\tau:t}^{HV} := [d_{t-\tau:t}, v_{t-\tau:t}]$ ), and a context vector ( $C_t := [X_t^{FV}, X_t^{TL}, TOD_t]$ ) including states of its front vehicle ( $X_t^{FV} := [r_t, \dot{r}_t]$ ), TLs ( $X_t^{TL} := [P_t, T_t]$ ), and time of day ( $TOD$ ) to a subsequent longitudinal acceleration of HV ( $a_t^{HV}$ ). The intuition behind the selected input features ( $X_t := [X_{t-\tau:t}^{HV}, X_t^{FV}, X_t^{TL}, TOD_t]$ ) is as follows :

**Distance to traffic light ( $d_t$ ), Longitudinal speed ( $v_t$ )** each represents a longitudinal distance of a HV to a TL that the HV is approaching or departing from and the longitudinal speed of the HV. They are essential features which greatly impacts behavior of vehicles. For example, a HV approaching a TL in red phase travels slowly when it is close to the TL, whereas it can travel fast when it is far

away from the TL.  $d_x > 0$  means that the HV is approaching the TL (upstream), and  $d_x < 0$  indicates that it's departing from the TL (downstream). We assume  $v_x \geq 0$ .

**Range and range-rate ( $r_t, \dot{r}_t$ )** each represents the relative longitudinal position and speed of the FV compared to the position and speed of a HV. We assume  $r_x > 0$ , meaning that the FV is always ahead of the HV. Note, due to the availability of our dataset (which only reported FV information), a rear or a side vehicle was not considered. However, one can trivially extend our model to include them.

**Phase and timing of traffic light ( $P_t, T_t$ )** represents the phase of a TL (G,Y,R) that a HV is subject to and the time elapsed since the last phase change ( $T_t \geq 0$ ).  $T_t$  accounts for transient behaviors of human drivers at phase shifts. For example, a vehicle approaching a TL in a red phase with a small  $T_t$ , meaning that the phase has just shifted to red, may not be traveling slowly whereas a vehicle approaching a TL with a large  $T_t$  is likely to travel slow or at a stop.

**Time of day ( $TOD$ )** represents the time of day as elapsed hours since midnight ( $0 \leq TOD < 24$ ).  $TOD = 0$ , and  $TOD = 12$  each indicates midnight and noon. The macroscopic traffic characteristics including congestion, and speed differ considerably depending on  $TOD$  as evidenced in studies including [21]. The selection of  $TOD$  is an attempt to incorporate the macroscopic trend of the traffic.

Due to the stochastic and complex nature of human decision making in driving, a simple analytical model such as a linear or a physics-based model cannot accurately represent the nominal or probabilistic behaviors of human-drivers near traffic signals. Instead, we argue that the proposed model should be obtained through data-driven modeling, using deep learning methods on historical driving data.

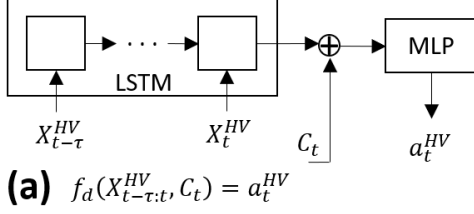
## D. Dataset

The dataset consists of 502,253 observations (samples) that 50 distinct vehicles have reported over a span of 27 months (Mar 2015 - July 2017) at a particular section of a road with a signalized intersection (SI). Each car reported its 10Hz GPS signals (coordinates, speeds, and heading angles) which then were used to calculate  $X_t^{HV}$ . The TL profile  $X_t^{TL}$  were obtained from a V2I communication device installed at the SI. The front-cameras mounted on the vehicles provided  $X_t^{FV}$ . In order to reduce the noise in  $X_t^{HV}, X_t^{FV}, a_t^{HV}$ , a least-square polynomial smoothing filter was used [22].

## E. Implementation Details

Both the deterministic ( $f_d$ ) and the probabilistic ( $f_p$ ) human policy models were implemented in Tensorflow-Keras. As depicted in Fig. 3, both models consist of a double-stacked LSTM which takes  $X_{t-\tau:t}^{HV}$  followed by a concatenation with the context vector  $C_t = [X_t^{FV}, X_t^{TL}, TOD_t]$ . The concatenated tensor is then fed into a multi-layer perceptron (MLP) for the deterministic model and a MDN for the

### Deterministic Policy ( $f_d$ ) Learning: RNN



### Probabilistic Policy ( $f_p$ ) Learning: RNN-MDN

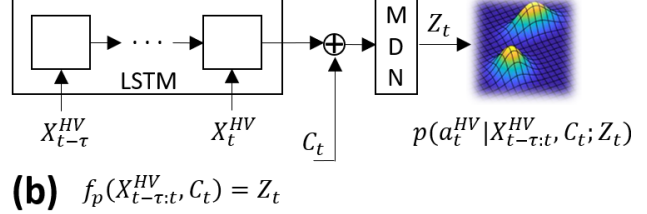


Fig. 3. The first part of the prediction framework: learning the policy. (a) a deterministic policy ( $f_d : [X_{t-\tau:t}^{HV}, C_t] \rightarrow a_t^{HV}$ ) is obtained by training the depicted model. (b) a probabilistic policy ( $f_p : [X_{t-\tau:t}^{HV}, C_t] \rightarrow Z_t$ ) by training the model based on LSTM-MDN as described in the figure.

probabilistic model. The MLP layer outputs  $a_t^{HV}$  whereas the MDN layer outputs the distribution parameters  $Z_t$ . Since Gaussian mixtures were used as the mixture network, the MDN outputs the following three parameter sets of the Gaussian mixture: mixture weights  $\pi_k$ , mean of components  $\mu_k$ , the variance of components  $\sigma_k$  for  $k = 1, 2, \dots, N$  and  $N$  is the number of components. We used  $N = 2$  for the yellow light dilemma scenario. Both models were trained on the same data using ADAM optimizer [23].

$f_d$  is learned by minimizing a loss function  $L_d$  which is a summation of mean squared error as described below.

$$L_d := \sum_{t=1}^T (a_t^{HV} - f_d(X_{t-\tau:t}^{HV}, C_t))^2 \quad (1)$$

$f_p$  is obtained by minimizing a loss function  $L_p$  which is a sum of a negative log-likelihood.

$$L_p := \sum_{t=1}^T -\log(p(a_t^{HV} | X_{t-\tau:t}^{HV}, C_t; Z_t)) \quad (2)$$

### III. TRAJECTORY FORECAST FRAMEWORK

As illustrated in Fig. 4, the proposed forecast framework consists of two parts. The first part of the framework is the off-line learning of the human policy models elaborated in Section II. The second part is where the trained models are used to obtain trajectory forecasts over the full prediction horizons. It is an iterative process, where we alternate one-step predictions of the policy models and propagations of vehicle dynamics. The one-step propagation of the longitudinal vehicle dynamics is done by utilizing a zero-order hold for discrete dynamics equations described in Eq. 3, 4, and 5.

$$v_{n+1} := v_n + a_n \Delta t_n \quad (3)$$

$$d_{n+1} := d_n + 0.5(v_{n+1} + v_n) \Delta t_n \quad (4)$$

$$X_{n+1}^{HV} = A_n X_n^{HV} + B_n a_n^{HV} \quad (5)$$

$$\text{where } A_n := \begin{bmatrix} 1 & \Delta t_n \\ 0 & 1 \end{bmatrix}, B_n := \begin{bmatrix} 0.5 \Delta t_n \\ \Delta t_n \end{bmatrix}, X_n^{HV} = \begin{bmatrix} d_n \\ v_n \end{bmatrix}.$$

Defining  $n = 0$ , and  $n = N$  as the index for  $t = 0$ , and  $t = T$ , the trajectory forecast over the prediction horizon  $t = [0, T]$  are obtained by propagating Eq. 5 from  $n = 0$  to  $n = N - 1$ :

$$\begin{aligned} X_N^{HV} &= \prod_{k=0}^{N-1} A_k X_0^{HV} + \prod_{k=1}^{N-1} A_k B_0 a_0^{HV} + \prod_{k=2}^{N-1} A_k B_1 a_1^{HV} \\ &\quad + \dots + A_{N-1} B_{N-2} a_{N-2}^{HV} + B_{N-1} a_{N-1}^{HV} \\ &= \prod_{k=0}^{N-1} A_k X_0^{HV} + \prod_{k=1}^{N-1} A_k B_0 f(X_{-n\tau+1:0}^{HV}, C_0) \quad (6) \\ &\quad + \dots + B_{N-1} f(X_{N-n\tau:N-1}^{HV}, C_{N-1}) \\ &:= F(X_{1:N-1}^{HV}, X_{-n\tau+1:0}^{HV}, C_{0:N-1}, \Delta t_{0:N-1}) \end{aligned}$$

where  $f$  can either be  $f_d$  or  $S(f_p)$ .  $S$  is a function which returns a sample  $a_t^{HV}$  according to the pdf of  $Z_t$  (In case of a unimodal Gaussian distribution,  $Z_t = [\mu_t, \sigma_t]$  and  $a_t^{HV} \sim N(\mu_t, \sigma_t^2)$ ).  $\tau, n\tau$  each indicates input sequence length in time, and in the number of steps.

As described in Eq. 6,  $X_N^{HV}$  is a function ( $F$ ) of  $[X_{1:N-1}^{HV}, X_{-n\tau+1:0}^{HV}, C_{0:N-1}, \Delta t_{0:N-1}]$ . The second term  $X_{-n\tau+1:0}^{HV}$  is obtained at  $t = 0$ , and the last term  $\Delta t_{0:N-1}$  can simply be pre-determined at the prediction time based on a required time resolution. Obtaining  $C_{0:N-1}$  at the prediction time ( $t = 0$ ) is the main challenge, due to uncertainties in  $X_{1:N-1}^{FV}, X_{1:N-1}^{TL}$ . A simple way to get away with the uncertainties is to simply design the model to forecast trajectories ( $X_{0:T}^{HV}$ ) conditioned on only the observed states  $[X_{-\tau:0}^{FV}, X_{-\tau:0}^{TL}]$ . An example is a model with many-to-many RNN that takes a sequence of past states and returns a sequence of future states. However, this approach cannot solve the forecasting problem we elaborated in the previous sections and in Fig. 2.

As briefly mentioned, the key idea is to remove the uncertainty by utilizing the future phases and timings of TMs obtained through vehicle-to-infrastructure communications. With the access to the future states of TMs,  $X_{1:N-1}^{TL}$  can be obtained at the prediction time. The remainder is then  $X_{1:N-1}^{FV}$ , which is predicted based on a variant of the human policy model  $f_d$ . Specifically, we train another human policy model  $f_d^{NoFV} : [X_{N-n\tau:N}^{HV}, C'_N] \rightarrow a_N^{HV}$  with  $C'_N := [X_{N-n\tau:N}^{TL}, TOD_N]$  taking  $X_N^{FV}$  out of the context. After the off-line learning of  $f_d^{NoFV}$  is done, we apply the iterative process described early in this section on FV to obtain  $X_{1:N-1}^{FV}$  via Eq. 6 with  $f_d^{NoFV}$ . Once  $[X_{1:N-1}^{FV}, X_{1:N-1}^{TL}]$  are calculated, the resulting trajectory forecast  $X_{1:N}^{HV}$  can be obtained. Note,  $X_{1:N}^{HV}$  can simply be forecast using  $f_d^{NoFV}$  as well. We conducted an ablation study (elaborated in Section IV) on  $f_d, f_d^{NoFV}$  and the other two models ( $f_d^{NoTL}, f_d^{NoFVTL}$ ) which each represents a model where  $X^{TL}$  and  $[X^{FV}, X^{TL}]$  are taken out of the context.

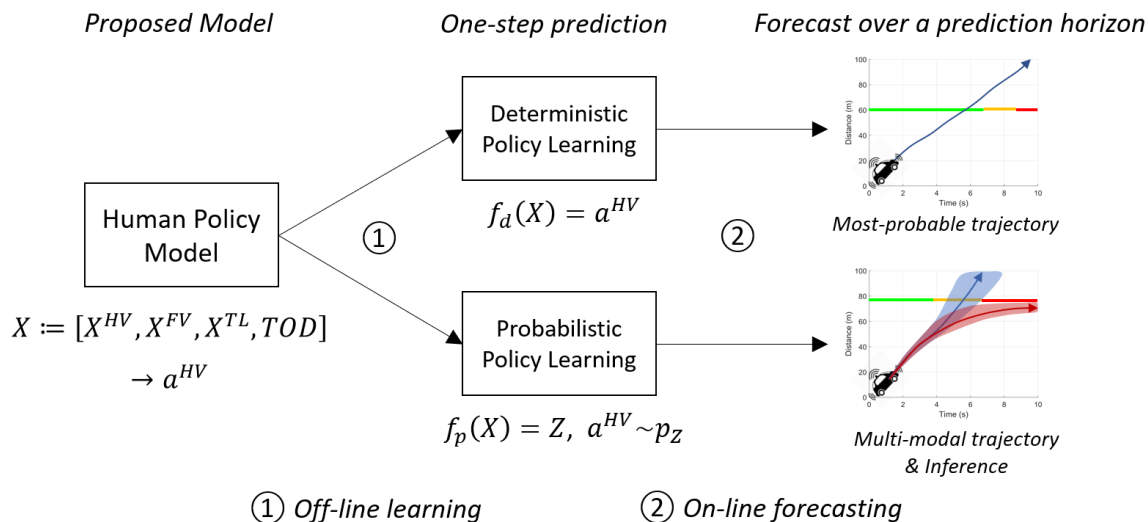


Fig. 4. The framework for the trajectory predictions is divided into two steps. The first step is to train the proposed policy model on a dataset based on two different approaches: deterministic and probabilistic learning (off-line). The second step is to predict the trajectories of target vehicles by iterative predictions of human policies and propagations of the longitudinal vehicle dynamics over the prediction horizon (on-line).

For the probabilistic human policy model, the probability of the resulting trajectory forecast  $p(X_{1:N}^{HV})$  can be estimated using the chain rule of probability, which factorizes the joint distribution over  $N$  separate conditional probabilities:

$$p(X_{1:N}^{HV} | X_{-n_\tau+1:0}^{HV}, C_{0:k-1}, \Delta t_{0:k-1}) = \prod_{k=1}^N p(X_k^{HV} | X_{1:k-1}^{HV}, X_{-n_\tau+1:0}^{HV}, C_{0:k-1}, \Delta t_{0:k-1}) \quad (7)$$

As opposed to the deterministic forecasting where the most-probable trajectory is obtained, a resulting trajectory is a sample from a probability distribution. While we can estimate the probability of a trajectory forecast via Eq. 7, the probability density function for  $X_t^{HV}$  needs to be numerically estimated since the distribution parameter  $Z_t$  is obtained via an arbitrarily complex neural network. Thus, we utilize Monte Carlo Simulation to obtain the samples (roll-out trajectories) and kernel density estimation to approximate the probability density functions of the samples.

#### IV. RESULTS

This section consists of 4 sub-sections. In section IV-A, we present the resulting trajectory forecasts for 4 examples sampled from our dataset to visualize the impact of  $X^{TL}$ . Furthermore, we demonstrate that utilization of phases and timings of TLs help the proposed model to accurately forecast long-term trajectories. In section IV-B, we discuss a set of metrics to evaluate the performance of trajectory forecasts and support an ablation study that is elaborated in section IV-C. The ablation study was designed to test the 4 variants of our deterministic models ( $f_d, f_d^{NoFV}, f_d^{NoTL}, f_d^{NoFVTL}$ ) on the test set (total 3,111 sample episodes of the scenarios discussed in Table I). In section IV-D, we demonstrate how our probabilistic prediction algorithm can be utilized to tackle a scenario with competing policies. Specifically, the yellow-light dilemma zone scenario is discussed.

##### A. Impact of $X^{TL}$ in trajectory forecasts

In order to investigate the impact of  $X^{TL}$ , we first train 4 variants of the deterministic policy models, and those 4 models are each used to compute the trajectory forecasts over a fixed prediction horizon via Eq. 6. The four policy models are  $f_d, f_d^{NoFV}, f_d^{NoTL}, f_d^{NoFVTL}$ , named depending on which features are used as the context  $C$ . Denoting  $C^{mode}$  as the context input for a deterministic policy model  $f_d^{mode}$ ,  $C^{NoFVTL} := [TOD], C^{NoTL} := [X^{FV}, TOD], C^{NoFV} := [X^{TL}, TOD]$ .

Fig. 5, 6 presents the trajectory forecasts for 4 examples (1 RG, 1 YR, 2 GYR scenarios) sampled from our dataset. The four trajectories that are depicted in each scenario represents ground-truth, three  $X_{0:T}^{HV}$  each from  $f_d, f_d^{NoFV}$ , and  $f_d^{NoTL}$ .

The sample on the left of Fig. 5 is similar to the motivational example in Fig. 2. At  $t = 0$ , the driver was stopped at a red phase. We can reasonably guess that a model without  $X_{0:5s}^{TL}$  is likely to forecast the vehicle to stay put. As expected, the forecast from  $f_d^{NoTL}$  (pink) failed to  $X^{HV}$  accurately, whereas the other two models were able to produce forecasts close to the ground-truth.

The right plot of Fig. 5 is a scenario YR where the driver slowed down approaching the intersection. Given  $P_0 = Y$  and that the vehicle was cruising ( $v_0 = 15$ ),  $f_d^{NoTL}$  forecast the vehicle to maintain the speed, causing the prediction errors to grow over time. The other two models  $f_d, f_d^{NoFV}$  which use  $X_{0:5s}^{TL}$  took account for the phase shift at  $t = 2.4s$ , and accurately forecast how the driver would react to the shift.

On the other hand, Fig. 6 describes scenarios that are longer (15s), and span a full cycle of phases (GYR). The first example on the left describes a scenario where the vehicle was initially at a stop due to a queue formed at the entrance of the intersection. Given the green phase observed at  $t = 0$ ,  $f_d^{NoTL}$  (pink) predicted that the queue will be dissipated soon and the vehicle will start to move in the future. However, what really happened was that the phase shifted to red



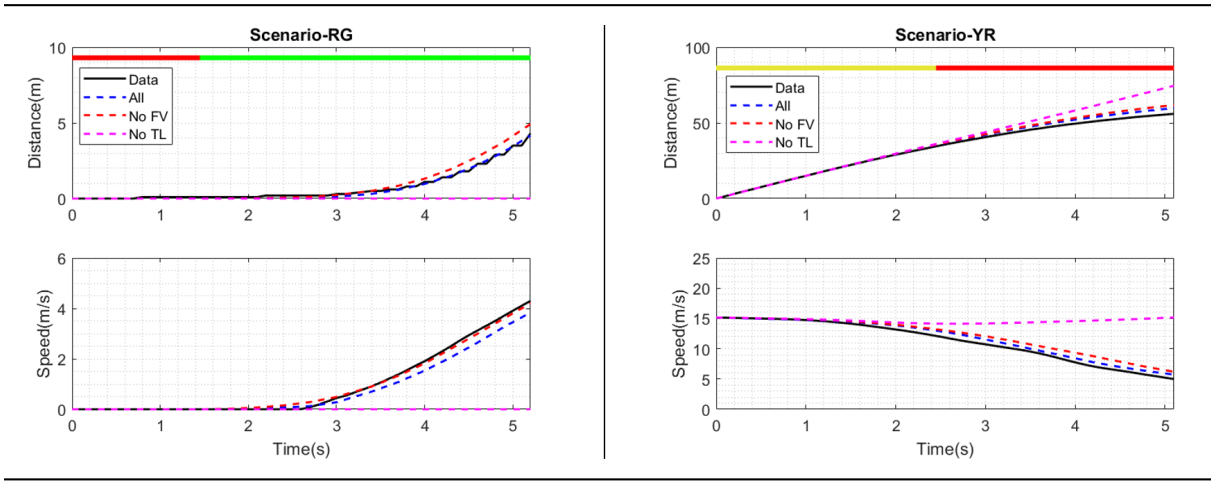


Fig. 5. Four trajectories (longitudinal position, speed) shown in the plot each represents ground-truth (black), three  $X_{0:5s}^{HV}$  obtained using  $f_d$  (Blue),  $f_d^{NoFV}$  (Red), and  $f_d^{NoTL}$  (Pink) for a scenario RG(left) and YR(right). 2s of history (omitted in the plot) were used to forecast trajectories 5s into the future.

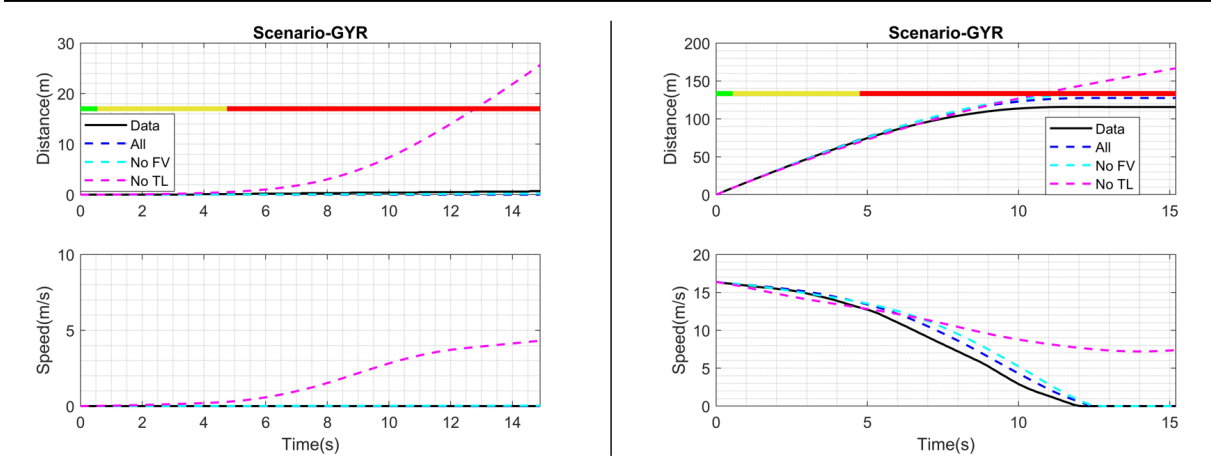


Fig. 6. Four trajectories for two examples of scenario GYR. 2s of history (omitted in the plot) were used to forecast trajectories 15s into the future  $X_{0:15s}^{HV}$ .

shortly, made the vehicle stay put (ground-truth). Note, the two models which utilized  $X_{0:15s}^{TL}$  were able to accurately forecast the trajectory over the 15 seconds horizon.

The second example of Fig. 6 is another GYR scenario, but with the vehicle initially approaching the intersection at  $v_0 = 16(m/s)$ .  $f_d^{NoTL}$  predicted that the vehicle will **cross** the intersection, given  $P_{t=0} = G$ . In reality, the vehicle made a stop before the intersection. Again,  $f_d, f_d^{NoFV}$  accommodated the future phases and timings of TL, successfully predicted that the vehicle would make a stop before the intersection.

As demonstrated, the impact of  $X^{TL}$  is significant: uncertainties in  $X^{TL}$  can cause high prediction errors, especially in long-term predictions. The results suggest that the existing forecasting methods can perform poor without the knowledge of future  $X^{TL}$ , highlighting why the problem is critical and needs to be solved. The proposed models are the solutions to the problem: the models which utilize future  $X^{TL}$  are able to predict the reactions of human drivers to TLs in diverse scenarios and greatly improve the accuracy of the forecasts.

## B. Evaluation metrics

For the evaluation of the trajectory forecasts, we used the following three metrics: mean absolute error (MAE), time weighted absolute error (TWAE), absolute deviation at the end of the prediction window (ADN) defined in Eq. 8, 9, and 10, where  $\hat{X}_k^{HV}, X_k^{HV}$  represents the  $k$ th-step forecast  $X$  and ground truth  $X$ .

$$MAE := \frac{\sum_{k=1}^N |\hat{X}_k^{HV} - X_k^{HV}|}{N} \quad (8)$$

$$TWAE := \frac{\sum_{k=1}^N (t_k |\hat{X}_k^{HV} - X_k^{HV}|)}{\sum_{k=1}^N t_k} \quad (9)$$

$$ADN := |\hat{X}_N^{HV} - X_N^{HV}| \quad (10)$$

We used  $\forall k: \Delta t_k = 0.2s, \tau = 2s$  (history). For the scenario with a prediction window  $T = 5s$  (or  $t_N = 5s$ ), the last index  $N$  is 25.

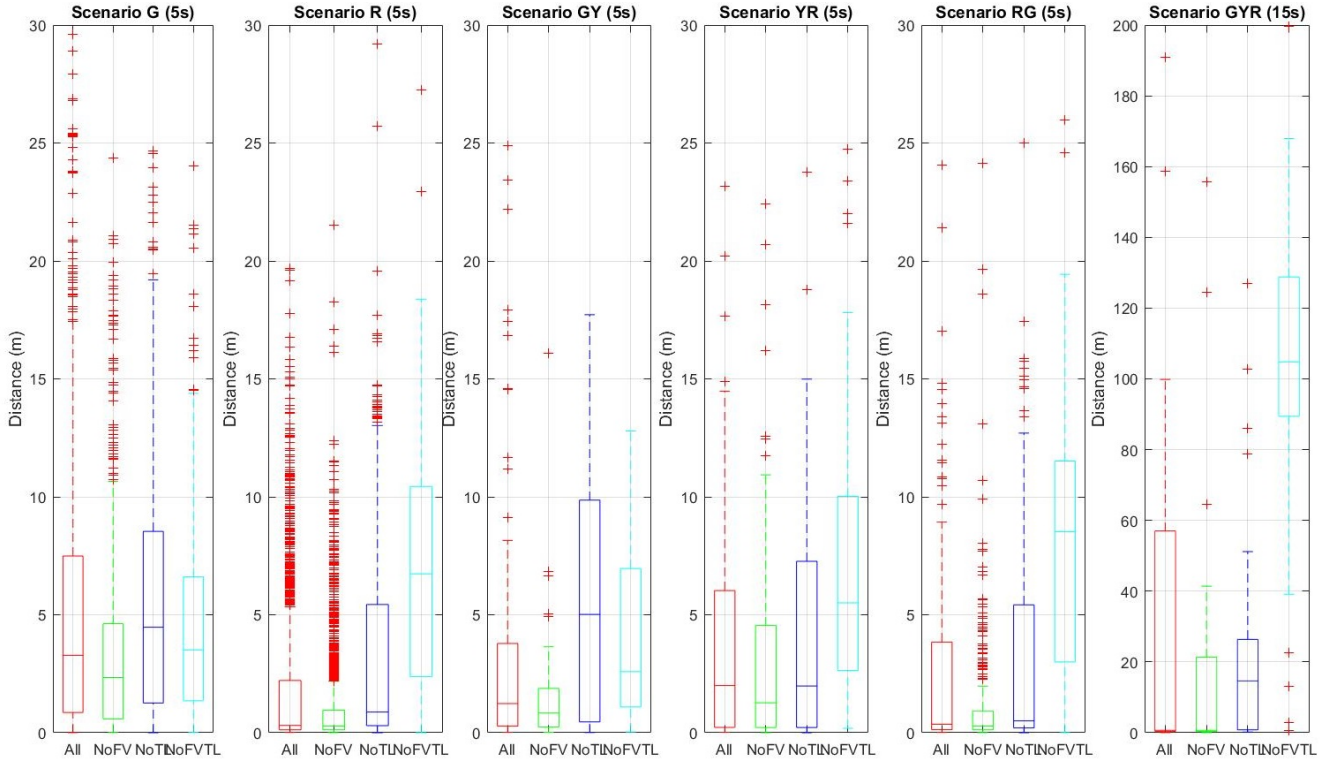


Fig. 7. An ablation study conducted on the test set depicted as a boxplot of positional prediction errors in ADN for 6 scenarios. All, NoFv, NoTL, NoFVTL each represents trajectory forecasts with  $f_d, f_d^{NoFV}, f_d^{NoTL}, f_d^{NoFVTL}$ . The prediction window is  $T = 15s$  for scenario GYR, and  $T = 5s$  for others.

### C. Ablation Study

The goal of the ablation study is to investigate the impact of  $X^{TL}$  in the trajectory forecast problem and evaluate the proposed models quantitatively. We first present Fig. 7, an evaluation on ADN for the four models ( $f_d, f_d^{NoFV}, f_d^{NoTL}, f_d^{NoFVTL}$ ) on the test set. The sample size for the scenarios are 688(G), 1909(R), 68(GY), 81(YR), 362(RG), 32(GYR), totalling 3,111 sample episodes. Note, the scenario Y is not depicted due to the inconsistent and short prediction horizon. We observed that the phase Y usually lasts anywhere between 2.5s to 4s. The first 2s are used as inputs, which means the prediction horizon for the scenario Y is only 0.5s to 2s. Second, we present the results on the performance evaluation of the four models on MAE, TWAE, and ADN on the same test set. Table. II, and III each serves the result for position and velocity errors.

ADN has the largest error among the three metrics (the magnitude of error:  $MAE < TWAE < ADN$ ). Fig. 7 depicts a box plot for ADN. In a box plot, the top and bottom edges of the box, the band inside the box each represents the 1st, 3rd quartiles, and the median. The ends of the whisker extend to the extreme data that are not considered outliers, and the outliers are indicated by '+'. As shown in Fig. 7, across all scenarios, the two models  $f_d, f_d^{NoFV}$  which utilizes  $X^{TL}$  outperform the other two models  $f_d^{NoTL}, f_d^{NoFVTL}$  which don't take advantage of the future phases and timings information. Interestingly, the winner is not  $f_d$ , but it is  $f_d^{NoFV}$ , which performs the best on all characteristics of boxplot including

the 1st, 3rd quartiles, the median, and the upper limit of the extreme points. Our interpretation is that the exclusion of  $X^{FV}$  increases the prediction accuracy, due to the uncertainty in  $X_{t>0}^{FV}$ .

The numbers presented in Table. II, III agree with the results from Fig. 7 across all scenarios.  $f_d^{NoFV}$  is the winner for almost all metrics, or at least on par with  $f_d$ . In summary, the knowledge of future states of traffic lights significantly increase the accuracy of trajectory forecasts, as evidenced in the ablation studies: trajectory forecasts with the winner model have roughly 2-6 times smaller (position) MAE, TWAE, ADN for  $T = 5s$  scenarios (G, R, GY, YR, RG), and roughly 9-21 times smaller MAE, TWAE, ADN for  $T = 15s$  scenario (GYR), compared to trajectory forecasts via  $f_d^{NoTL}$ .

### D. Probabilistic Prediction

The outliers observed in Fig. 7 occur mostly because of edge cases and competing policies. Examples of the edge cases include a driver approaching the intersection in  $P_{vt} = R$  with high speed and executing a sudden break right before the entrance of the intersection rather than gradually slowing down it approaches the intersection. Another example is that a driver in the middle of the road in  $P_{vt} = G$  moving much slower than the average speed of the traffic for unknown reasons. The outliers occur from competing policies are exemplified by the yellow light dilemma scenario where a driver can either cross the intersection or stop before the intersection.

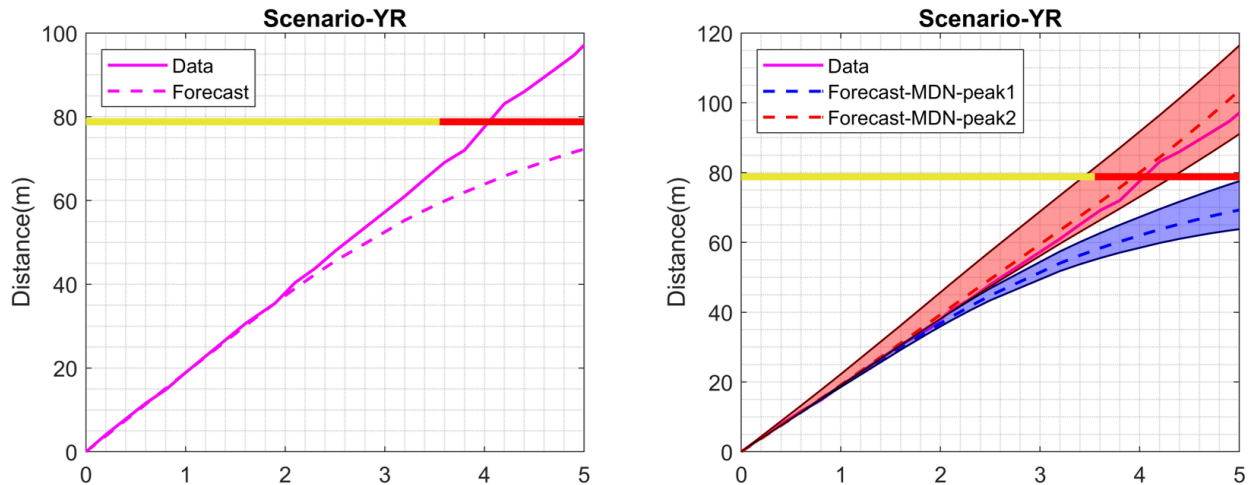


Fig. 8. A sample trip for the yellow light dilemma scenario. The left plot highlights the limitation of the most-probable trajectory. The right plot shows that the proposed probabilistic models are able to forecast the two competing policies. The trajectories  $\forall t : p(d_t) \geq 0.01$  are illustrated.

Fig. 8(a) describes a sample trip observed in our dataset that represents the yellow light dilemma scenario. As shown in the figure, the most-probable trajectory forecast obtained via  $f_d^{NoFV}$  predicts that the vehicle would make a stop before the intersection, however, the driver crossed the intersection even after the phase shifted to red.

This is where the proposed probabilistic human policy models come in handy. The probabilistic models are capable of reproducing multi-modal distributions, thus capture the other competing policy (*cross*). The probabilistic forecasts are not only capable of capturing competing policies, but also able to reason the uncertainties of the forecasts and provide contexts on the predictions as the probabilities of the forecasts can be estimated.

We argue that the deterministic models are still valuable: the solutions are simple, cost-efficient, and easy to interpret. They can serve as nominal trajectories of human drivers in situations that can be approximated uni-modal or described with a normal distribution. The nominal trajectories can be used in a trajectory planning algorithm which does not allow uncertainties in surrounding environments.

For the scenarios with 5s prediction horizon, the time to compute a most-probable trajectory forecast is less than 10msecs on a single-core personal laptop with i7-6500U 2.50GHz CPU, and 8GB RAM without a parallelization. However, it takes several seconds (5-10s for 1,000 rollout trajectories) to construct the pdf for the probabilistic forecasts on the same machine due. One can significantly reduce the time via parallel computing (GPU).

## V. CONCLUSION

One of the remaining challenges for autonomous driving is how to accurately predict the trajectories of vehicles near traffic lights in various states of traffic lights. In this paper, we elaborated the trajectory forecast problem where the existing methods can perform poorly. We address this gap by proposing a novel approach where we leverage the future

states of traffic lights. Specifically, we propose deterministic and probabilistic human policy models which simulate how human drivers take actions in terms of accelerations depending on diverse driving scenarios near TLs. We train the models on a real-world naturalistic driving dataset and utilize them to obtain longitudinal trajectory forecasts based on a simple idea: the utilization of the future traffic signal phase and timing information obtained from V2I communications. The human policy models are learned using a recurrent neural network, and a gaussian-mixture based Mixture Density Network. We show that the utilization of future phases and timings of TLs can significantly improve the quality of the trajectory forecasts through the ablation study. The ablation study also highlights that the proposed methods are comprehensive models that tackle the diverse scenario of the trajectory forecast problem described in Table. I. It is worth noting that the proposed models are not necessarily replacements for other state-of-the-art trajectory forecasting models, but rather the great addition to any method that concerns vehicle trajectory forecasting near TLs.

The predicted trajectories then can be utilized for various applications in decision makings, trajectory plannings, and controls of a host vehicle (either a self-driving car or a human-driven car). Our current interests include an extension of the work presented in [24]; we plan to improve the performance of the energy-optimal planning algorithm presented in [24] by leveraging our trajectory forecast framework to model other vehicles in the scenes. In conclusion, the proposed human policy model helps us to better understand and predict behaviors of human drivers in the vicinity of traffic lights and can be leveraged to improve autonomous drivings in urban city driving, including decision-making, planning, and control of host vehicles.

## ACKNOWLEDGMENT

The authors would like to thank the University of Michigan Transportation Research Institute for access to the SPMD dataset.



TABLE II

Ablation study on **position** errors with average MAE, TWAE, ADN. Prediction horizon is 15s for GYR and 5s for others. The lower a metric is, the better. The numbers from the best performing model are marked in **bold**.

Scenario	MAE(m)				TWAE(m)				ADN(m)			
	All	NoFV	NoTL	NoFVTL	All	NoFV	NoTL	NoFVTL	All	NoFV	NoTL	NoFVTL
G	1.18	<b>0.78</b>	1.35	1.19	1.86	<b>1.21</b>	2.16	1.78	3.28	<b>2.34</b>	4.47	3.51
R	0.16	<b>0.15</b>	0.38	1.79	0.21	<b>0.20</b>	0.56	2.98	0.31	<b>0.28</b>	0.88	6.74
GY	0.53	<b>0.41</b>	1.26	0.82	0.77	<b>0.54</b>	2.06	1.31	1.24	<b>0.84</b>	5.01	2.59
YR	1.18	<b>0.69</b>	0.86	1.01	1.60	<b>0.93</b>	1.32	1.42	2.00	<b>1.27</b>	1.98	2.29
RG	0.17	<b>0.14</b>	0.22	2.28	0.24	<b>0.19</b>	0.31	3.80	0.36	<b>0.28</b>	0.50	8.53
GYR	<b>0.445</b>	<b>0.445</b>	4.11	32.40	<b>0.567</b>	0.568	6.82	51.16	<b>0.694</b>	<b>0.694</b>	14.65	104.81

TABLE III

Ablation study on **velocity** errors with average MAE, TWAE, ADN. Prediction horizon is 15s for GYR and 5s for others.

Scenario	MAE(m/s)				TWAE(m/s)				ADN(m/s)			
	All	NoFV	NoTL	NoFVTL	All	NoFV	NoTL	NoFVTL	All	NoFV	NoTL	NoFVTL
G	0.70	<b>0.46</b>	0.97	0.75	1.02	<b>0.65</b>	1.41	1.07	1.48	<b>0.94</b>	2.28	1.51
R	<b>0.005</b>	<b>0.005</b>	0.17	1.44	0.007	<b>0.006</b>	0.22	2.29	0.010	<b>0.009</b>	0.29	4.10
GY	0.39	<b>0.15</b>	1.11	0.53	0.54	<b>0.20</b>	1.78	0.79	0.87	<b>0.27</b>	3.08	1.21
YR	<b>0.367</b>	0.374	0.53	1.01	<b>0.47</b>	0.52	0.71	1.42	<b>0.59</b>	0.69	0.89	2.29
RG	0.007	<b>0.005</b>	0.10	1.68	0.010	<b>0.007</b>	0.14	2.63	0.02	<b>0.01</b>	0.22	4.52
GYR	0.015	<b>0.014</b>	1.26	6.78	<b>0.018</b>	0.020	1.86	9.80	0.030	<b>0.029</b>	2.60	14.13

## REFERENCES

- [1] N. Lee, W. Choi, P. Vernaza, C. B. Choy, P. H. Torr, and M. Chandraker, "Desire: Distant future prediction in dynamic scenes with interacting agents," in *Proceedings of the IEEE Conference on Computer Vision and Pattern Recognition*, 2017, pp. 336–345.
- [2] J. Li, H. Ma, and M. Tomizuka, "Interaction-aware multi-agent tracking and probabilistic behavior prediction via adversarial learning," *arXiv preprint arXiv:1904.02390*, 2019.
- [3] N. Rhinehart, K. M. Kitani, and P. Vernaza, "R2p2: A reparameterized pushforward policy for diverse, precise generative traffic forecasting," in *Proceedings of the European Conference on Computer Vision (ECCV)*, 2018, pp. 772–788.
- [4] A. Alahi, K. Goel, V. Ramanathan, A. Robicquet, L. Fei-Fei, and S. Savarese, "Social lstm: Human trajectory prediction in crowded spaces," in *Proceedings of the IEEE conference on computer vision and pattern recognition*, 2016, pp. 961–971.
- [5] R. Chandra, U. Bhattacharya, A. Bera, and D. Manocha, "Traffic: Trajectory prediction in dense and heterogeneous traffic using weighted interactions," in *Proceedings of the IEEE Conference on Computer Vision and Pattern Recognition*, 2019, pp. 8483–8492.
- [6] A. Gupta, J. Johnson, L. Fei-Fei, S. Savarese, and A. Alahi, "Social gan: Socially acceptable trajectories with generative adversarial networks," in *Proceedings of the IEEE Conference on Computer Vision and Pattern Recognition*, 2018, pp. 2255–2264.
- [7] C. R. Bennett and R. Dunn, "Driver deceleration behavior on a freeway in new zealand," *Transportation Research Record*, no. 1510, 1995.
- [8] J. Wang, K. K. Dixon, H. Li, and J. Ogle, "Normal deceleration behavior of passenger vehicles at stop sign-controlled intersections evaluated with in-vehicle global positioning system data," *Transportation research record*, vol. 1937, no. 1, pp. 120–127, 2005.
- [9] C. Sun, X. Shen, and S. Moura, "Robust optimal eco-driving control with uncertain traffic signal timing," in *2018 Annual American Control Conference (ACC)*. IEEE, 2018, pp. 5548–5553.
- [10] R. Akçelik and D. Biggs, "Acceleration profile models for vehicles in road traffic," *Transportation Science*, vol. 21, no. 1, pp. 36–54, 1987.
- [11] G. Bham and R. Benekohal, "Development, evaluation, and comparison of acceleration models," in *81st Annual Meeting of the Transportation Research Board, Washington, DC*, vol. 6, 2002.
- [12] ATS, "Acceleration/deceleration profiles at urban intersections," *Transit New Zealand Australasian Traffic Surveys*, 1990.
- [13] P. P. Dey, S. Nandal, and R. Kalyan, "Queue discharge characteristics at signalised intersections under mixed traffic conditions," *European Transport*, vol. 55, no. 7, pp. 1–12, 2013.
- [14] J. Park, D. Li, Y. L. Murphey, J. Kristinsson, R. McGee, M. Kuang, and T. Phillips, "Real time vehicle speed prediction using a neural network traffic model," in *The 2011 International Joint Conference on Neural Networks*. IEEE, 2011, pp. 2991–2996.
- [15] B. Jiang and Y. Fei, "Vehicle speed prediction by two-level data driven models in vehicular networks," *IEEE Transactions on Intelligent Transportation Systems*, vol. 18, no. 7, pp. 1793–1801, 2016.
- [16] K. Fadhoun, H. Rakha, and P. Eng, "A vehicle dynamics model for estimating typical vehicle accelerations 2," *Transportation Research Record: Journal of the Transportation Research Board*, vol. 35, no. 36, p. 37, 2015.
- [17] M. Treiber, A. Hennecke, and D. Helbing, "Congested traffic states in empirical observations and microscopic simulations," *Physical review E*, vol. 62, no. 2, p. 1805, 2000.
- [18] P. G. Gipps, "A behavioural car-following model for computer simulation," *Transportation Research Part B: Methodological*, vol. 15, no. 2, pp. 105–111, 1981.
- [19] C. M. Bishop, "Mixture density networks," Citeseer, Tech. Rep., 1994.
- [20] T. J. Gates, D. A. Noyce, L. Laracuente, and E. V. Nordheim, "Analysis of driver behavior in dilemma zones at signalized intersections," *Transportation Research Record*, vol. 2030, no. 1, pp. 29–39, 2007.
- [21] G. Oh, D. J. Leblanc, and H. Peng, "Vehicle energy dataset (ved), a large-scale dataset for vehicle energy consumption research," *arXiv preprint arXiv:1905.02081*, 2019.
- [22] R. W. Schafer *et al.*, "What is a savitzky-golay filter," *IEEE Signal processing magazine*, vol. 28, no. 4, pp. 111–117, 2011.
- [23] D. P. Kingma and J. Ba, "Adam: A method for stochastic optimization," *arXiv preprint arXiv:1412.6980*, 2014.
- [24] G. Oh and H. Peng, "Eco-driving at signalized intersections: What is possible in the real-world?" in *2018 21st International Conference on Intelligent Transportation Systems (ITSC)*. IEEE, 2018, pp. 3674–3679.